Response sensitivity of a semisubmersible floating offshore wind turbine to different wind spectral models

Response sensitivity of a semisubmersible floating offshore wind turbine to different wind spectral models

R M Putri [1], C Obhrai[1], J B Jakobsen[1]

[1]Department of Mechanical and Structural Engineering and Material Science, University of Stavanger, 4026, Stavanger, Norway

rieska.m.putri@uis.no

Abstract. Previous research on the OC3 spar floating offshore wind turbine (FOWT) has shown the sensitivity of the yaw and side-side modes' load and motion responses to different atmospheric conditions. Using the same baseline turbine of the OC3 spar wind turbine for a semisubmersible floater (OC4), this study investigates the load and motion responses of such offshore wind turbine for neutral and unstable atmospheric conditions. The effect of different levels of wind spatial coherence associated with two different wind spectral models for neutral conditions (Kaimal and Mann) are studied for the same turbulence intensity levels. An increase of 18% in the tower torsional moment fatigue damage equivalent load (DEL) is observed for the wind inflow with the weakest coherence (Mann spectral model), compared to the DELs under turbulent wind inflow with the highest coherence (Kaimal spectral model). Unstable atmospheric conditions are also simulated based on the Pointed-Blunt spectral model derived from FINO1 wind measurement. The yaw mode of the semisubmersible wind turbine is found to be the response component most affected by the variation in atmospheric stability conditions. A 28% higher fatigue DEL for the tower torsional moment is observed for very unstable atmosphere than the DELs under neutral atmospheric conditions.

1. Introduction

In recent years, the bottom fixed offshore wind industry has matured to the point that subsidies are no longer required. As we develop sites farther from shore and in deeper waters, floating offshore wind turbines will become the next generation of the offshore wind power producing devices. Floating substructures are offered as an alternative solution enabling cost reduction and installation simplicity compared to the bottom-fixed substructures in the deep water offshore. The two well-known floating offshore wind farms currently built in Europe, the Hywind Scotland and the WindFloat Atlantic, adopt a spar floater and a semisubmersible floater. A FOWT structure must be designed to withstand offshore environmental loads, primarily waves, current, and wind during its lifetime. While the overall responses of a FOWT floater under wave loading are well understood from the oil and gas designs, its responses with respect to wind loading however are still a topic of active research.

The FOWT floaters carry not only the dead loads from the wind turbine, but also the rotating blade harmonic loads which are affected by the turbulent wind conditions on the rotor. In particular, the low-frequency part of the turbulent wind contributes to loading in the rotating rotor frequencies [1]. Moreover, the interaction between each degree of freedom (DOF) of the floater motions and the rotor's responses due to the wind inflow is also a concern. When a FOWT is pitching, the resulting rotor tilt may cause yaw loads on the FOWT, specifically for a spar-type floater [1]. A spar FOWT has been shown to have an increased yaw response when exposed to a less coherent turbulent wind inflow [2, 3,

4]. A less spatially-coherent wind inflow for lateral separations results in higher twisting moments about the spar wind turbine's vertical axis and thus creates greater yaw loads and motion responses [2, 3]. Furthermore, different levels of turbulent wind energy associated with various atmospheric conditions are also found to affect the yaw load and motion of a spar-type wind turbine [5, 6]. The two aspects of turbulent wind flow (spatial coherence and turbulent wind energy content) significantly contribute to the yaw responses since a spar-type FOWT has low resistance to yaw. Motivated by previous studies on a spar-type floating wind turbine [2, 3, 4, 5] and the fact that a semisubmersible FOWT also corresponds to long eigen-periods susceptible to wind excitation, we aim to investigate the response sensitivity of a semisubmersible FOWT to the variation in turbulent wind inflow. In the present study the responses of the DeepCwind from the OC4 project [7] is investigated under different turbulent wind inflow conditions.

2. Turbulent wind models

Turbulent wind is a random process which is complex to simulate. In common engineering design of wind turbines, standard guidelines such as IEC 61400-1 [8] are commonly used. In this standard, two wind spectral models are recommended for numerical simulations of turbulent wind fields for neutral atmospheric stability conditions: the Kaimal Spectra [9] with an Exponential Coherence, and the Mann Spectral Tensor Model [10]. A neutral atmospheric stability condition indicates no vertical temperature flux in the atmosphere, a condition not necessarily prevailing in the offshore atmospheric [9]. Over the ocean, there often exists significant temperature discrepancies between the sea water surface and the air, which results in enhanced vertical mixing under unstable atmospheric stability conditions [11]. The present offshore wind turbine design guidelines take into account wind spectral models for neutral atmospheric conditions only. A wind spectral model such as the Pointed-Blunt [12], which was derived based on wind measurement data from an offshore site, can be used to represent non-neutral atmospheric conditions.

The turbulent wind fields used in this study are simulated by focusing on two different aspects of turbulent wind: (1) variation in the spatial coherence, and (2) variation in the atmospheric stability. Variation in the spatial coherence is represented by simulated wind fields comparing the Kaimal and the Mann spectral models [8] for neutral atmospheric stability conditions. The Kaimal and Mann spectral models are equivalent in terms of turbulent energy, but not the spatial coherence [8]. Variation in the atmospheric stability is represented by wind fields simulated using the Pointed-Blunt spectral model [12] for progressively decreasing atmospheric stability from neutral to very unstable, assuming fixed spatial coherences for all stabilities.

2.1. Kaimal spectra

The Kaimal spectra was derived based on measured wind data in Kansas [9] and widely used to simulate turbulent wind fields. The adopted formulation of the single-sided one-point Kaimal spectra in the IEC 61400-1 is expressed as [8]:

$$\frac{fS_i(f)}{\sigma_i^2} = \frac{\frac{4fL_i}{U_{hub}}}{\left(1+\frac{6fL_i}{U_{hub}}\right)^{5/3}} \tag{1}$$

where
f: frequency (Hz)
i: velocity component index (u: longitudinal, v: lateral, and w: vertical)
S_i: velocity spectrum for each component i
σ_i: standard deviation of velocity component i (m/s), detailed in ref. [8]
L_i: integral length scale of velocity component i (m), detailed in ref. [8]
U_{hub}: mean wind speed at hub height (m/s)

The one-point spectra given in Eq. (1) is paired with an exponential coherence to compute the surrounding points' spectral properties of the u- wind component [8]:

$$Coh_{uu}(f,\Delta) = exp\left[-12\sqrt{\left(\frac{f\,\Delta}{U_{hub}}\right)^2 + \left(\frac{0.12\,\Delta}{L_u}\right)^2}\right] \quad (2)$$

where Δ is the separation distance, either lateral or vertical (m). As stated in the IEC 61400-1, Eq. (2) is applicable only for the longitudinal wind component u-, while coherence formulation for the lateral (v) and vertical (w) components are not given. In the TurbSim guideline [13], identity coherence is recommended for v- and w- components. However, in the absence of validated coherence values for v- and w- components, the present study utilizes Eq. (2) as the coherence formulation for v- and w- components as well.

2.2. Mann spectral tensor model

The Mann spectral tensor implies isotropic von Kármán spectra as the initial condition, and the presence of wind shear allows the isotropic flow transforms into anisotropic flow with time as the eddies' structure is stretched until they break [10]. The velocity component spectra for the Mann spectral tensor model as given in the IEC 61400-1 is [8]:

$$\frac{fS_i(f)}{\sigma_i^2} = \frac{{\sigma_{iso}}^2}{\sigma_i^2}\left(\frac{4\pi\ell f}{U_{hub}}\right)\Psi_{ij}\left(\frac{2\pi\ell f}{U_{hub}}\right) \quad (3)$$

where

Ψ_{ij}: autospectrum/cross-spectrum as a function of spectral tensor components, detailed in ref. [8]

σ_i^2: component variance (m^2/s^2)

σ_{iso}: 0.55 σ_u (m/s)

ℓ: 0.8 Λ_u, taken as 33.6 m

To account for the anisotropy, the shear parameter γ is added to the spectral tensor model so the model has three representative parameters in total: $\alpha\epsilon^{2/3}$ (a measure of the turbulent kinetic energy dissipation rate), ℓ, and γ [10]. A fit to the Kaimal spectral model in Eq. (1) gives the value of 3.9 for the shear parameter γ [8]. The coherence is then calculated as [10]:

$$Coh_{ij}(f,\Delta_y,\Delta_z) = \frac{\left|\Psi_{ij}(f,\Delta_y,\Delta_z)\right|^2}{S_i(f)S_j(f)} \quad (4)$$

with Δ_y and Δ_z are the separation distances respectively in the lateral and vertical directions with respect to the incoming wind inflow. The resulting coherences for lateral separations from Eq. (4) are much lower than those given in Eq. (2), especially at frequencies lower than 0.2 Hz [4]. The same applies to the involved co-coherences, which concern the in-phase, simultaneous action of turbulence across the considered separations.

2.3. Pointed-Blunt spectra

The Pointed-Blunt spectral model was derived based on two-year measured wind data from FINO1 platform [12]. The model is a one-point spectra presented in a similar form to the Kaimal spectra, except it is made up by a low-frequency part and a high-frequency part. Each of the parts has two floating parameters which depend on the atmospheric stability. The parameters are defined for the range of $-2 < \zeta < 2$; where ζ is the stability parameter = z/L_m, z is the measured height (m) and L_m is the Obukhov length (m). For the considered stability, from very stable (ζ=2) to neutral (ζ=0) and then very unstable (ζ=-2), the turbulent kinetic level increases progressively [12]. The Pointed-Blunt spectra is given as [12]:

$$\frac{fS_i(f)}{u_*^2} = \frac{{a_1}^i f}{\left(1 + {b_1}^i f\right)^{5/3}} + \frac{{a_2}^i f}{\left(1 + {b_2}^i f^{5/3}\right)} \quad (5)$$

where a_1^i, a_2^i, b_1^i, b_2^i are the floating parameters for different velocity component i (u: longitudinal, v: lateral, w: vertical), and u_* is the friction velocity (m/s). Here, the spectral model in Eq. (5) is paired with the exponential coherence given in Eq. (2) for u-, v-, and w- velocity components, which is adopted for all considered stability conditions.

3. Numerical simulations

Coupled SIMO-Riflex included in the Simulation Workbench for Marine Application (SIMA) is used as the main numerical simulation tool. By utilizing SIMO-Riflex and simulated wind fields as input, the load and motion responses of the OC4-DeepCwind wind turbine corresponding to different turbulent wind inflow conditions are computed and analyzed. Turbulent wind fields are generated accordingly for all load cases presented in Table 1 by means of TurbSim [13] for Kaimal spectral model, Mann Turbulence Generator [14] for Mann spectral model, and windSimFast [15] for Pointed-Blunt spectral model. These wind fields are produced in the form of moving 'turbulence box' in the direction of the incoming longitudinal wind u- component for the coupled SIMO-Riflex simulations.

3.1. Load case

The load cases (LCs) are divided into LC 1 (variation in the wind spatial coherence) and LC 2 (variation in the atmospheric stability). The turbulent intensity (TI) input for LC 1 are adopted to match the simulated values for LC 2a. Table 1 presents the simulated TI and other input values for all load cases. It can be observed from Table 1 that the TI values for LC 1 are close to the target values in LC 2a. A uniform mean wind profile is used for all load cases in Table 1. Additional simulations were performed for LC 2 by applying a stability-corrected logarithmic mean wind profile. This is discussed further in Subsection 4.5. A constant irregular wave input for all load cases is added to SIMA simulations using the JONSWAP spectra with significant wave height H_s = 4 m, peak period T_p = 8 s, and peakedness parameter γ = 3.3. The selected wave peak period is far shorter than the OC4-DeepCwind's first six eigen-periods. To minimize the uncertainties, each load case is simulated with six different random seeds and the simulation time step is taken as 0.01 s for a continuous 3600 s duration. Three mean wind speeds at hub height (U_{hub}) are considered for each load case given in Table 1, 8 m/s (below rated), 11.4 m/s (rated), and 15 m/s (above rated).

Table 1. Load case.

Load case	Wind model	Atmospheric stability	Coherence function	$\alpha\epsilon^{2/3}$ for 8, 11.4, 15 m/s	Input TI [%] for 8, 11.4, 15 m/s	Simulated TI [%] for 8, 11.4, 15 m/s
1a	Kaimal	Neutral (ζ=0)	Eq. (2)	-	5.95, 6.08, 6.16	5.77, 5.93, 6.03
1b	Mann[1]	Neutral (ζ=0)	Eq. (4)	0.00956, 0.0203, 0.036	5.95, 6.08, 6.16	5.83, 5.95, 6.01
2a	Pointed-Blunt	Neutral (ζ=0)	Eq. (2)	-		5.95, 6.08, 6.16
2b		Weakly unstable (ζ=-0.407)				6.0, 6.11, 6.18
2c		Unstable (ζ=-0.815)				6.51, 6.61, 6.67
2d		Very unstable (ζ=-1.63)				7.6, 7.74, 7.83

[1]other input parameters: ℓ=33.6m, γ=3.9

3.2. DeepCwind characteristics

The OC4-DeepCwind is the phase II of the Offshore Code Comparison Collaboration Continuation (OC4) project which adopts the NREL 5 MW offshore baseline turbine with a semisubmersible floater [7]. For shortness, the properties of the DeepCwind are not shown here but can be found in Robertson

et al. [7]. Figure 1a illustrates the DeepCWind semisubmersible wind turbine model in SIMA. The NREL 5 MW offshore baseline turbine has the cut-in, rated, and cut-out wind speeds of 3, 11.4, and 25 m/s respectively. The hub height is 90 m above mean seawater level and the rotor diameter is 126 m. The cut-in and rated rotor speeds are 6.9 and 12.1 rpm respectively. The simulated eigen-frequencies of the first eight modes of the OC4-DeepCwind compared to the OC4 code comparison are given in Figure 1b and show a good agreement.

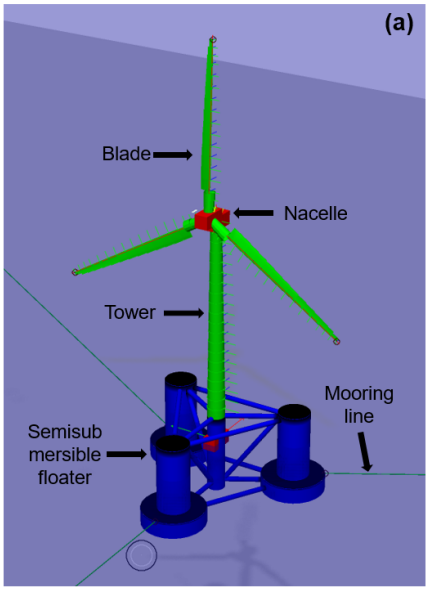

(b)

Mode	Simulated [Hz]	OC4 code comparison [7] in [Hz]
Surge	0.00875	0.0089-0.0105
Sway	0.00867	0.0089-0.0105
Yaw	0.0125	0.012-0.016
Pitch	0.038	0.0385-0.046
Roll	0.04	0.0385-0.049
Heave	0.055	0.054-0.056
1st tower side-side	0.44	0.38-0.5
1st tower fore-aft	0.45	0.38-0.5

Figure 1. (a) DeepCWind wind turbine model in SIMA and (b) the simulated eigen-frequencies.

4. Result

Structural response of the DeepCwind wind turbine with respect to the different turbulent wind inflows is studied in terms of the fatigue DEL. The 1-hour output time series of the considered stress resultants (in this case bending and torsional moment) are quantified as DEL and calculated by assuming an equivalent number of cycles n_{eq} of 10^7 during a 20-year lifetime:

$$DEL = \left(\frac{\Sigma N_i {S_i}^m}{n_{eq}} \right)^{1/m} \tag{6}$$

where N_i is the total number of cycles causing failure due to repeated stresses with a magnitude of S_i. The number of stresses in each bin is obtained from the Rainflow counting method [16]; m is the Wöhler exponent, here taken as 3 for steel material (tower) and 12 for fiberglass material (blade). The moments and the related fatigue damage are evaluated for the tower base fore-aft, tower base side-side, and the blade root flap-wise. The tower base and tower top torsional moments are also studied. In addition, the displacement responses (motions) are presented in the form of minimum, maximum, and standard deviation. The resulting force and displacement responses of the DeepCwind are discussed separately, when exposed to different turbulent wind conditions for neutral atmospheric stability with variable coherences (LC 1) and for different atmospheric stability conditions with constant coherences (LC 2).

4.1. Fore-aft response

It is noted that the tower base fore-aft moment DELs are increasing with wind speed. The tower base fore-aft moment power spectral density (PSD) plots are given in Figure 1 for the rated wind speed (11.4 m/s). The highest response is found for LC 2d (very unstable atmospheric condition) and is reduced as

turbulence level decreases as the atmospheric stability tends to neutral conditions (from LC 2d to LC 2a, Figure 2). Figure 2 shows that the tower base fore-aft moment response from LC 1b (Mann spectral model) are of a similar magnitude to those in LC 2d even though LC 1b considers neutral stability. However, the observed DEL difference between the highest (LC 2d) and the lowest (LC 2a) averaged tower base fore-aft DELs is only 3.4% (noted at 8 m/s), which is negligible. The highest excitation for the tower fore-aft moment is observed at the wave frequency as shown in Figure 2. In our simulations, the wave input was kept the same, and as a result there is negligible variation at the wave excitation for different load cases. Figure 3 shows the platform pitch response and it is noted that the platform pitch standard deviation is neither affected by variation in the spatial coherence nor influenced by variation in the turbulent energy content.

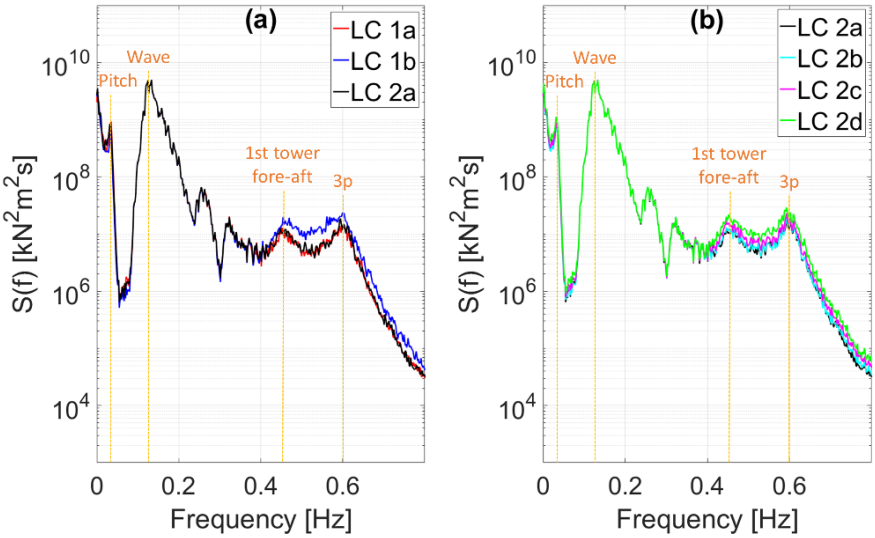

Figure 2. PSD of tower base fore-aft moment at the rated wind speed (11.4 m/s) for: (a) neutral stability and (b) different stability conditions.

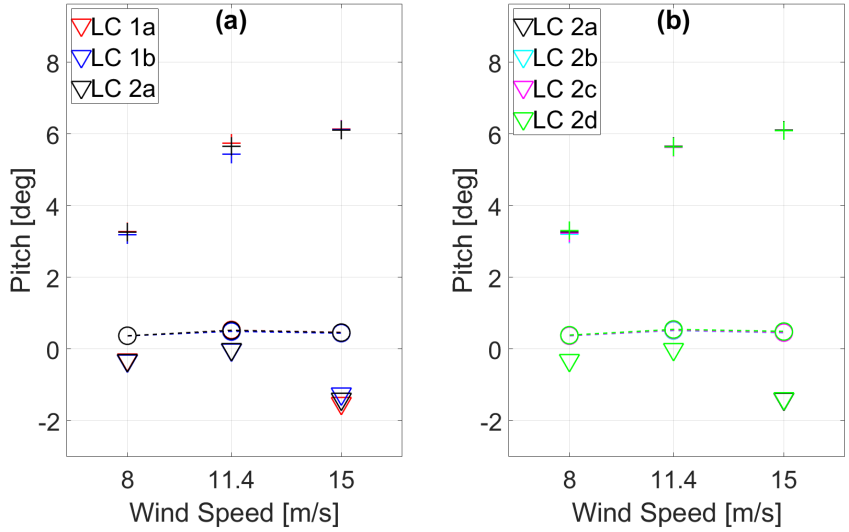

Figure 3. Platform pitch for: (a) neutral stability and (b) different stability conditions. Triangles indicate the minimum values, circles indicate the standard deviations, and plus indicate the maximum values.

4.2. Side-side response

Figure 4 gives the normalized DELs and Figure 5 gives the PSD response at 8 and 11.4 m/s of the tower base side-side for all load cases. Figure 4 shows that the DELs are the lowest at the rated wind speed (11.4 m/s) which might be caused by the influence of blade controller transition from a constant pitch angle to variable pitch angle. We note at wind speeds below rated, the tower base side-side DELs are primarily excited in the 1st tower side-side (Figure 5a). As the wind speeds approach rated and above, the excitation in the 1st tower side-side is reduced and excitation at the 3p frequency appears (Figure 5b). The highest averaged DEL is observed for LC 2d (very unstable conditions) and decreases as turbulence level decreases with the atmospheric conditions tend towards neutral (LC 2d to LC 2a, Figure 4b). However the DELs from LC 1b (Mann spectral model) are of similar magnitude to the DELs from LC 2d. The observed difference between the highest (LC 1b) and the lowest (LC 1a) averaged tower base side-side DEL is 30% at 15 m/s (Figure 4a).

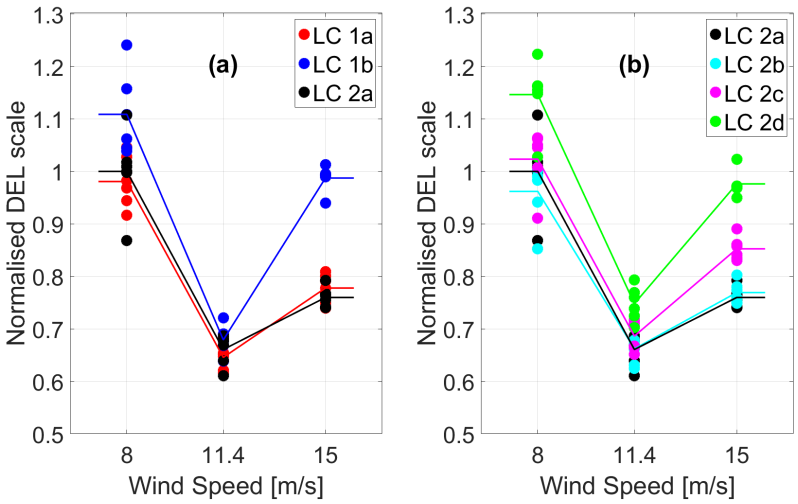

Figure 4. Normalized DELs of tower base side-side moment for: (a) neutral stability and (b) different stability conditions. Normalized by the values of LC 2a at 8 m/s.

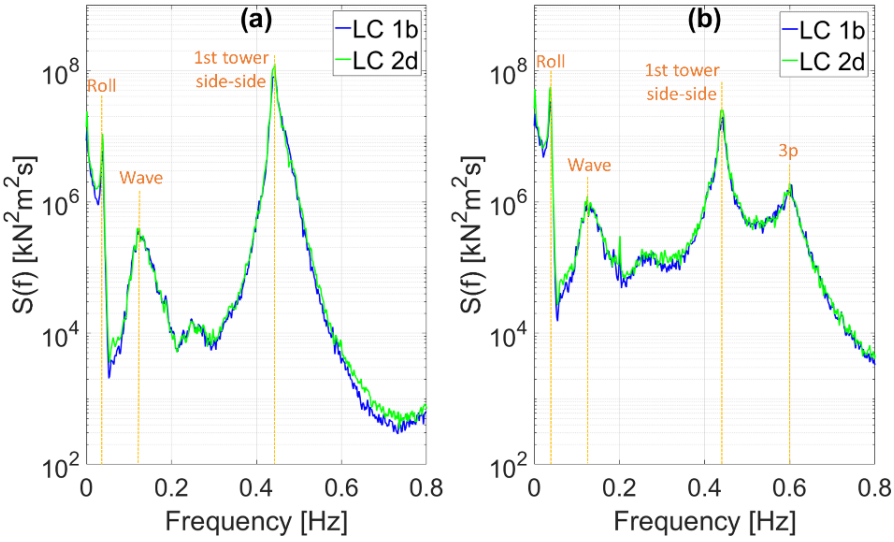

Figure 5. PSD of tower base side-side moment at: (a) 8 m/s and (b) 11.4 m/s.

Figure 6 presents the platform sway response and it shows a clear trend of sway response both with variation in the spatial coherence (Figure 6a) and the variation in atmospheric stability (Figure 6b). A less coherent turbulent wind inflow (LC 1b) results in larger sway, whereas the platform sway is decreasing gradually as the atmospheric conditions tend towards neutral (from LC 2d to LC 2a). The platform roll response is not shown here but it is noted that the platform roll is decreasing gradually from very unstable (LC 2d) to neutral conditions (LC 2a), while no clear trend is observed for variation in the spatial coherence (LC 1).

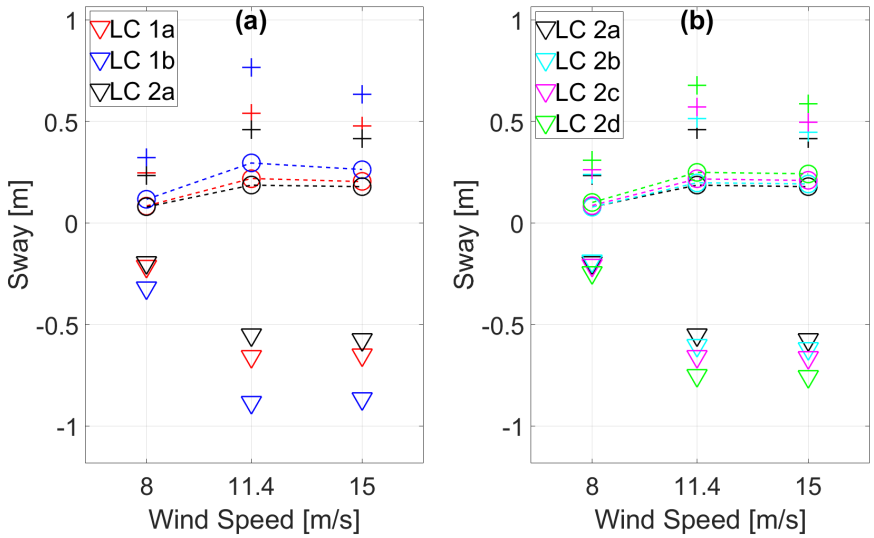

Figure 6. Platform sway for: (a) neutral stability and (b) different stability conditions. Triangles indicate the minimum values, circles indicate the standard deviation, and plus indicate the maximum values.

4.3. Yaw/torsion response

It is observed that the characteristics of the tower base torsional moment and the tower top torsional moment responses are very similar, therefore only tower top torsional moment is discussed here. In Figure 7, the normalized tower top torsional moment DELs are noted to increase with wind speed. Again, the highest averaged DEL is observed for LC 2d (very unstable conditions) and decreasing as the stability tends towards neutral atmospheric stability (from LC 2d to LC 2a, Figure 7b).

The DELs from LC 1b (Mann spectral model) are higher than the DELs under unstable conditions (LC 2c), due to the lower lateral coherence and the associated higher twisting moments about the turbine's vertical axis. This effect is also apparent for the platform yaw responses as presented in Figure 8, where the standard deviations from LC 1b even exceed the standard deviations from LC 2d. The difference between the highest (LC 2d) and the lowest (LC 2a) averaged tower top torsional moment DELs is 28% at 15 m/s (Figure 7b).

4.4. Blade root flap-wise bending

The blade root flap-wise moment DELs are seen to increase with wind speed. The difference between the highest (LC 1a) and the lowest (LC 1b) averaged blade root flap-wise moment DELs is 5.5% at 15 m/s. This is likely due to a more coherent wind inflow (for both vertical and lateral separations) in the LC 1a (Kaimal spectral model) compared to the wind flow defined by the Mann spectral model (LC 1b). With respect to the variation in the atmospheric stability (LC 2), the averaged DEL values do not vary significantly.

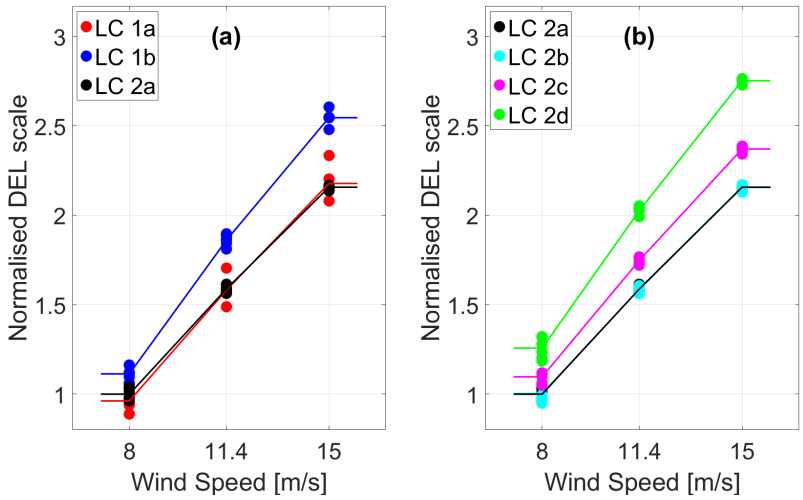

Figure 7. Normalized DELs of tower top torsional moment for: (a) neutral stability and (b) different stability conditions. Normalized by the values of LC 2a at 8 m/s.

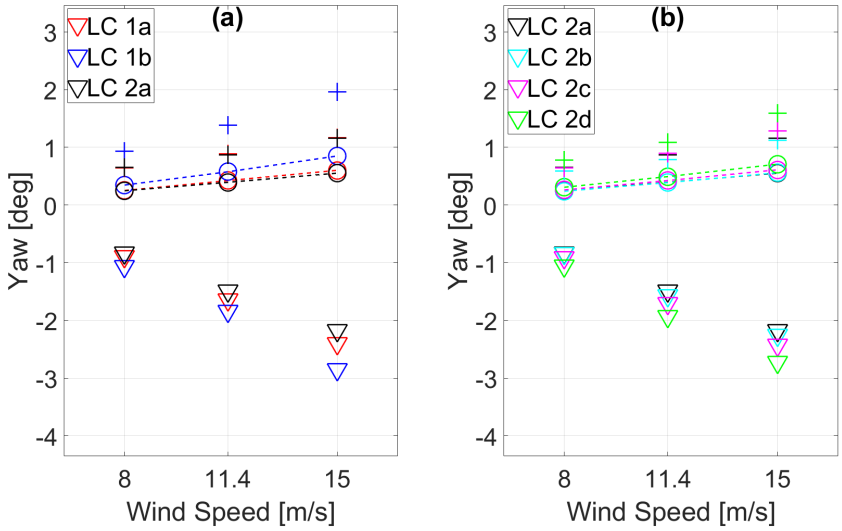

Figure 8. Platform yaw for: (a) neutral stability and (b) different stability conditions. Triangles indicate the minimum values, circles indicate the standard deviation, and plus indicate the maximum values.

4.5. Influence of the stability-corrected mean wind profile

The use of stability-corrected mean wind profile for LC 2 results in similar platform motions as shown in Subsection 4.1 to 4.4. The associated DELs with the use of stability-corrected mean wind profile for LC 2 also give similar DEL values to the simulations with a uniform mean wind profile. However, the observed average DEL values are lower by up to 8% for the tower base side-side moment, tower base torsional moment, and tower top torsional moment than those described in Subsection 4.1 to 4.4. The average blade root flap-wise DELs are shown to be increasing by 1.5% with the inclusion of stability-corrected mean wind profile as the stability shifts from neutral to very unstable. This is in agreement with Kretschmer et al. [18] who studied the measured blade root flap-wise DEL response from Alpha Ventus wind farm located near FINO1 platform, where the wind model used in LC 2 is derived from. Nonetheless, the 1.5% increase is negligible as there is very little wind shear for very unstable

conditions. Mean wind profile contribution could be more significant under stable atmospheric conditions which are not addressed in the present study.

5. Discussion

We note that the yaw and side-side responses of the DeepCwind are affected by different turbulent wind fields in a similar manner to the spar Hywind wind turbine from the OC3 project studied previously [3, 5]. The observed similar sensitivity of the yaw and side-side modes could be because the OC4 DeepCwind and the OC3 Hywind share the same turbine, the NREL 5 MW offshore baseline. When a FOWT experiences yaw errors between the rotor axis and the incoming wind direction (in the present case due to the prominent rotor yawing), side-side induced loads are triggered [17]. Such side-side induced loads' variation is then dependent on the turbine's properties i.e. rotor mass as well as the floater resistance to roll. From this study, the DeepCwind platform's roll is seen to have smaller deviations than those studied for the Hywind turbine [5].

The platform heave responses of the DeepCwind show negligible variation with different turbulence conditions because waves are the governing load for the platform heave translation [3]. In the present study, the wave input is kept constant for all load cases, therefore such conclusion is observed.

6. Conclusion

The yaw and the side-side response of the OC4 DeepCwind are demonstrated to be sensitive to the variation in the different turbulent wind inflow conditions, related to the spatial coherence and the atmospheric stability. The side-side response is largely triggered by the rotor-wind yaw error due to the rotor yawing. Other response components are seen to be less sensitive to the studied turbulent wind conditions. An 18% increase in the tower torsional moment and 30% increase for the tower side-side moment averaged DELs are observed for the simulated responses using the Mann spectral model (weaker coherence) than the simulated responses using the Kaimal spectral model (higher coherence). A 28% increase in the tower torsional moment and 28% increase for the tower side-side moment averaged DELs are observed for the simulated responses under very unstable conditions than the values obtained from neutral conditions.

Acknowledgement

The authors would like to express their gratitude to Dr. Lene Eliassen and Dr. Etienne Cheynet for their guidance and valuable knowledge through the completion of this work.

References

[1] DNV GL 2018 *DNV GL-ST-0119 Floating wind turbine structures* (DNV GL)
[2] Godvik M 2016 Influence of Wind Coherence on the Response of a Floating Wind Turbine *NORCOWE Science Meets Industry Stavanger*
[3] Bachynski E E and Eliassen L 2019 The Effects of Coherent Structures on the Global Response of Floating Offshore Wind Turbines *Wind Energy* **22** 219–38
[4] Doubrawa P, Churchfield M J, Godvik M and Sirnivas S 2019 Load response of a floating wind turbine to turbulent atmospheric flow *Applied Energy* **242** 1588–99
[5] Putri R M, Obhrai C and Knight J M 2019 Offshore Wind Turbine Loads and Motions in Unstable Atmospheric Conditions *J. Phys: Conf. Ser.* **1356** 012016
[6] Knight J M and C. Obhrai 2019 The Infulence of an Unstable Turbulent Wind Spectrum on the Loads and Motions on Floating Offshore Wind Turbines *IOP Conf. Ser: Materials Science and Engineering* **700** 012005
[7] Robertson A et al. 2014 Offshore code comparison collaboration continuation within IEA wind task 30: phase II results regarding a floating semisubmersible wind system *American Society of Mechanical Engineers Digital Collection*
[8] IEC 2005 Wind energy generation systems, Part 1: Design requirements (Geneva: IEC)
[9] Kaimal J C and Finnigan J J 1994 *Atmospheric boundary layer flows: their structure and*

measurement (New York: Oxford University Press)
[10] Mann J 1994 The Spatial Structure of Neutral Atmospheric Surface-Layer Turbulence *Journal of fluid mechanics* **273** 141–68
[11] Krogsæter O and Reuder J 2014 Validation of Boundary Layer Parameterization Schemes in the Weather Research and Forecasting (WRF) Model under the Aspect of Offshore Wind Energy Applications-Part II: Boundary Layer Height and Atmospheric Stability *Wind Energy* **18** 769–82
[12] Cheynet E, Bogunovic J B and Reuder J 2018 Velocity Spectra and Coherence Estimates in the Marine Atmospheric Boundary Layer *Boundary-Layer Meteorology* **169** 429–60
[13] Jonkman J 2016 *TurbSim User's Guide: Version 2.00.00* (Golden: NREL)
[14] Larsen T J and Hansen A M 2019 *How 2 HAWC2, the user's manual* (Risø: DTU Wind Energy)
[15] Cheynet E 2018 *Wind Field Simulation* [Online, accessed January 2019]
[16] Tatsuo E, Koichi M, Kiyohumi T, Kakuichi K and Masanori M 1974 Damage evaluation of metals for random or varying loading—three aspects of rain flow method *Mechanical Behavior of Materials* 21–4
[17] Kretschmer M, Schwede F, Guzmán R F, Lott S and Cheng P W 2018 Influence of atmospheric stability on the load spectra of wind *J. Phys: Conf. Ser.* **1037** 052009
[18] Jonkman J and Matha D 2010 *Quantitative comparison of the responses of three floating platforms No. NREL/CP-500-46726* (Golden: NREL)